

# A metabolomics approach shows that catechin-enriched green tea attenuates ultraviolet B-induced skin metabolite alterations in mice

Eun Sung Jung · Hye Min Park · Kyung-Eun Lee · Jung-Hoon Shin · Sukyeong Mun · Jeong Kee Kim · Sang Jun Lee · Kwang-Hyeon Liu · Jae-Kwan Hwang · Choong Hwan Lee

Received: 24 April 2014 / Accepted: 17 October 2014 / Published online: 26 October 2014  
© Springer Science+Business Media New York 2014

**Abstract** In this study, catechin-enriched green tea (CGT) administration significantly attenuated ultraviolet (UV) B-induced mouse skin alterations, i.e., increases in wrinkle formation, thickness, erythema, and transepidermal water loss, and decreases in hydration, elasticity, and collagen fiber content. The metabolites in the mouse skin after UVB irradiation and CGT administration were profiled using comprehensive MS-based metabolomics techniques such as ultra-performance liquid chromatography-quadrupole time-of-flight-mass spectrometry (TOF-MS), gas chromatography-TOF-MS, and NanoMate tandem-MS. From these analysis, we reveal that Normal, UVB-irradiated, and UVB-

irradiated with CGT administrated groups clearly discriminated from each other in partial least squares-discriminant analysis models, and CGT administration attenuated UVB-induced alteration of skin metabolites such as lysophospholipids, fatty acids, ceramides, amino acids, organic compounds, lipids, and nucleobases. Among them, purine nucleobases (inosine and hypoxanthine), ascorbic acid, and lactose were remarkably influenced by CGT administration, which indicated that these metabolites could be biomarkers to explain CGT effects on UVB-irradiated skin. Our results suggested that CGT administration was effective in reducing the levels of UVB-induced alterations of numerous mouse skin metabolites, and these metabolites were might highly relevant to observed changes in skin conditions.

**Electronic supplementary material** The online version of this article (doi:10.1007/s11306-014-0743-x) contains supplementary material, which is available to authorized users.

E. S. Jung · H. M. Park · C. H. Lee (✉)  
Department of Bioscience and Biotechnology, Konkuk University, 120 Neungdong-ro, Gwangjin-gu, Seoul 143-701, Republic of Korea  
e-mail: chlee123@konkuk.ac.kr

K.-E. Lee · S. Mun · J.-K. Hwang (✉)  
Department of Biotechnology, Yonsei University, 50 Yonsei-ro, Seodaemun-gu, Seoul 120-749, Republic of Korea  
e-mail: jkhwang@yonsei.ac.kr

J.-H. Shin · K.-H. Liu  
College of Pharmacy and Research Institute of Pharmaceutical Sciences, Kyungpook National University, Daegu 702-701, Republic of Korea

J. K. Kim · S. J. Lee  
Food Research Institute, AmorePacific R&D Center, Yongin 446-729, Republic of Korea

J.-K. Hwang  
Department of Biomaterials Science and Engineering, Yonsei University, Seoul 120-749, Republic of Korea

**Keywords** Catechin-enriched green tea · Metabolite profiling · Mouse skin · Ultraviolet B

## 1 Introduction

Ultraviolet (UV) radiation is a major environmental factor contributing to the development of various skin diseases. The UV spectrum is divided into three regions depending on the wavelength; short-wave UVC (200–290 nm), mid-wave UVB (290–320 nm), and long-wave UVA (320–400 nm). In particular, UVB radiation penetrates the whole epidermal and dermal layers of the skin to a depth of approximately 160–180  $\mu\text{m}$  (Nichols and Katiyar 2010). Exposure to UV radiation can result in immunosuppression, oxidative damage, connective tissue damage, and premature aging in the skin (Kligman et al. 1985; Brenneisen et al. 2002).

Green tea (*Camellia sinensis*) is one of the most popular beverages enjoyed worldwide. The major catechins found

in green tea include epicatechin (EC), epicatechin-3-gallate (ECG), epigallocatechin (EGC), and epigallocatechin-3-gallate (EGCG). These have been shown to have a number of health benefits, such as prevention of cancer, cardiovascular disease, and neurodegenerative effects (Mukhtar and Ahmad 2000; Yang et al. 2009). Due to the strong antioxidant activities of green tea catechins, the photoprotective effects of these agents have also generated significant interest (Yang et al. 2009), and a number of studies have focused on the dermatological effects of green tea catechins against UV radiation. For example, Jeon et al. (2003) investigated the effect of dietary supplementation with catechins on cutaneous antioxidant enzymes in UVB-irradiated skin, and the molecular mechanisms underlying the effects of green tea catechin administration on UV radiation-induced skin damage also have been well studied (Vayalil et al. 2004; Meeran et al. 2009). Furthermore, a number of studies demonstrated greater beneficial health effects of catechin-rich green tea on various diseases such as diabetes and cardiovascular disease (Nagao et al. 2007; Huang et al. 2013). However, the use of a metabolite profiling approach to investigate the metabolite biomarkers responsible for the effect of catechin-enriched green tea (CGT) administration in UVB-irradiated mice has not yet been reported.

Metabolomics is an important field in the comprehensive study of small molecules in biological systems, such as tissues, cells, and organs. Metabolites are the final products of metabolic responses of living systems and represent biological biomarker candidates for disease states (Arakaki et al. 2008; Zhang et al. 2012). Previous mass spectrometry (MS)-based metabolomics studies on biological materials convincingly demonstrated that metabolomics can be useful for revealing biomarker candidates of diseases and restoring effects of active ingredients (Zhou et al. 2012; Kim et al. 2013; Park et al. 2014). Therefore, the major objective of this study was to investigate the effect of CGT administration on UVB-induced metabolite changes in mouse skin using ultra-performance liquid chromatography-quadrupole-time-of-flight (UPLC-Q-TOF)-MS, gas chromatography (GC)-TOF-MS, and NanoMate tandem-MS.

## 2 Materials and methods

### 2.1 Chemicals and materials

Acetonitrile, dichloromethane (DCM), methanol, and water were obtained from Fisher Scientific (Pittsburgh, PA, USA). Formic acid, pyridine, methoxyamine hydrochloride, *N*-methyl-*N*-(trimethylsilyl)trifluoroacetamide (MSTFA), and standard compounds were purchased from Sigma Chemical

Co. (St. Louis, MO, USA). All chemicals were analytical grade. The CGT was obtained from AmorePacific Corp. (Yongin, Korea). The CGT contains considerable amount of catechins (27.58 %), including EGC (7.50 %), EC (2.56 %), EGCG (13.28 %), and ECG (4.24 %). In addition, chlorophyll (2.58 %), caffeine (6.03 %), and theanine (2.60 %) were contained.

### 2.2 Animal experiment

Female SKH-1 hairless mice (5 weeks old) were purchased from Orient Bio (Seongnam, Korea) and housed in environmentally controlled rooms ( $22 \pm 2$  °C,  $55 \pm 15$  % relative humidity, 12-h light/dark cycle) at Yonsei Laboratory Animal Research Center (YLARC; Seoul, Korea). All animal experiments were performed in accordance with the Korea Food and Drug Administration guidelines. Protocols were reviewed and approved by the Institutional Animal Care and Use Committee of the YLARC (Permit #: 2011-0081). After a 1-week acclimation, mice were fed a standard diet (Cargill Agri Purina; Seongnam, Korea) and water. The mice were randomly divided into 3 groups: Normal (NOR) group ( $n = 6$ ), UVB-irradiated (UVB) group ( $n = 7$ ), and UVB-irradiated with CGT administered (UVB + CGT) group ( $n = 7$ ). The UVB-irradiated groups were exposed to UVB radiation three times per week for 12 weeks, using the UV crosslinker CL-1000 M (UVP; Cambridge, UK). The CGT administered group was orally administered with 250 mg/kg CGT daily for 12 weeks with UVB exposure. UVB irradiation started with 75 mJ/cm<sup>2</sup> doses (1 minimal erythema dose, MED), and the doses were elevated weekly from 1 MED to 4 MED. During the experiment period, the body weight of mice were measured weekly and showed no difference among the groups (data not shown). After 12 weeks of experimenting, the mice were sacrificed and their dorsal skin samples were harvested and stored at  $-70$  °C.

### 2.3 Clinical and histological assessment

Skin wrinkles of hairless mice were copied using the Visioline VL 650 system (CK Electronics GmbH; Cologne, Germany). The skin replica represented the total area, number, length, and depth of the wrinkles. Erythema index, skin hydration, and transepidermal water loss (TEWL) were measured on the dorsal skin of hairless mice before sacrifice using Mexameter<sup>®</sup> 18, Corneometer<sup>®</sup> 825, and Tewameter<sup>®</sup> TM 300, respectively (CK Electronics GmbH). Epidermal thickness was visualized via hematoxylin and eosin (H&E) staining, and measured with a caliper. Masson's trichrome staining was used to evaluate collagen fibers in the dermis. Gross elasticity was calculated using the Cutometer device, representing the recovery

rate to the initial state. Changes in the amount of elastic fibers were also visualized by Verhoeff-van Gieson's staining. The stained sections were observed using an Eclipse TE2000U Microscope with twin CCD cameras (Nikon; Tokyo, Japan).

#### 2.4 Metabolite extraction from skin tissues

Metabolite profiling was performed on extracts of mouse skin tissues. Before solvent extraction, skin tissues (2 × 3 cm size) from the central dorsum of mice were finely chopped. For metabolite profiling, extraction from skin tissues were performed with 1 mL of methanol using MM400 mixer mill (Retsch®; Haan, Germany) with a frequency of 30 s<sup>-1</sup> for 20 min. After centrifugation (12,000 rpm, 4 °C, 10 min), the supernatant was filtered through a 0.2-µm polytetrafluoroethylene filter, and dried using a speed vacuum concentrator (Modulspin 31; Biotron, Korea). Dried samples were further analyzed by UPLC-Q-TOF-MS and GC-TOF-MS.

For ceramide analysis, the remaining pellets were re-extracted with 1 mL of solvent mixture (DCM:MeOH, 2:1) using an MM400 mixer mill with a frequency of 30 s<sup>-1</sup> for 20 min. After centrifugation (12,000 rpm, 4 °C, 10 min), the supernatant was filtered through a filter, and evaporated using a speed vacuum concentrator. Dried samples were further analyzed by NanoMate-LTQ.

#### 2.5 UPLC-Q-TOF-MS analysis

For the UPLC-Q-TOF-MS analysis, dried samples were re-dissolved with methanol. UPLC was performed on a Waters ACQUITY UPLC™ system (Waters Corp., Milford, MA, USA) equipped with a binary solvent delivery system, a UV detector, and an autosampler. Chromatographic separation was performed on a Waters ACQUITY BEH C18 column (i.d., 100 mm × 2.1 mm, 1.7 µm particle size; Waters Corp.) and the injection volume was 5 µL. The column temperature was set at 37 °C and the flow rate was 0.3 mL/min. The mobile phase consisted of 0.1 % v/v formic acid in water (A) and 0.1 % v/v formic acid in acetonitrile (B). The initial condition was 5 % B for 1 min and linearly increased to 55 % B over 4 min, and increased to 100 % B over 8 min. Total run time was 15 min, including re-equilibration of the column to the initial condition. For MS experiments, the Waters Q-TOF Premier (Micromass MS Technologies, Manchester, UK) was operated in negative ion modes with an *m/z* range of 100–1,000. The source temperature was set at 100 °C; the collision energy was set at 10 eV and the collision gas flow was 0.3 mL/min; the desolvation gas was set to 650 L/h at a temperature of 300 °C. The capillary voltage and sample cone voltage were set at 2.5 kV and 50 V, respectively. The V mode was used for the mass spectrometer and

data were collected in the centroid mode with a scan accumulation 0.2 s. Leucine enkephalin was used as reference lock mass (*m/z* 554.2615) by independent LockSpray interference.

#### 2.6 GC-TOF-MS analysis

Methoximation and silylation were performed for the GC-TOF-MS analysis. Methyloxime derivatives were obtained by dissolving the dry tissue extracts in 50 µL of methoxyamine hydrochloride (20 mg/mL in pyridine) for 90 min at 30 °C. After methoximation, samples were silylated for 30 min at 37 °C by adding 50 µL of MSTFA. GC-TOF-MS analysis was performed by using a Agilent 7890 gas chromatograph system (Agilent Technologies, Palo Alto, CA, USA) coupled with Agilent 7693 autosampler (Agilent Technologies) and equipped with Pegasus® HT TOF MS (LECO, St. Joseph, MI, USA) system. An Rtx-5MS column (i.d., 30 m × 0.25 mm, 0.25 µm particle size; Restek Corp., Bellefonte, PA, USA) was used with a constant flow of 1.5 mL/min of helium as carrier gas. One microliter aliquot of the sample was injected into the GC with split ratio of 5:1. The oven temperatures maintained at 75 °C for 2 min, followed by raised to 300 °C at 15 °C/min, and then, finally hold for 3 min. The temperatures of the front inlet and transfer line were 250 °C and 240 °C, respectively. The electron ionization was carried out at -70 eV and full scanning over a range of 50–1,000 *m/z* was used for mass data collection.

#### 2.7 Targeted ceramide analysis and data processing

To perform target ceramide analysis, we used an LTQ XL mass spectrometry (Thermo Fisher Scientific; West Palm Beach, FL, USA) equipped with a TriVersa NanoMate robotic nanoflow ion source (Advion Biosciences; Ithaca, NY, USA) and nanoelectrospray chips with spraying nozzles 5.5 µm in diameter. Chipsoft 8.3.2 software (Advion Biosciences) was used to control the ion source. The parameters were set for proper instrumental analysis including ionization voltage (-1.45 kV, negative mode), backpressure (0.4 psi), tube voltage (-100 V), and ion transfer capillary temperature (200 °C). Ten micro liter of the analyte was electrosprayed for more than 50 min. On the 96-well plate of the TriVersa NanoMate ion source, 10 µL of samples were loaded for analysis and then sealed with aluminum foil. Each sample was analyzed for 2 min. The data collection method performed a full scan (*m/z* 400–1,000) and a data-dependent MS/MS scan of the most abundant ions. Low resolution mode was used for scanning standard spectra with 30 eV CID voltage to obtain specific MS/MS fragmentation. All spectra were recorded using Thermo Xcalibur software (version 2.1; Thermo Fisher

Scientific). MS data from the ion trap mass spectrometer were aligned using MATLAB software (version 8.0; MathWorks; Natick, MA, USA).

## 2.8 Data processing and multivariate statistical analysis

The UPLC-Q-TOF-MS data were acquired with MassLynx software (version 4.1; Waters Corp.), and raw data files were converted into NetCDF format (\*.cdf) using the MassLynx DataBridge (version 4.1; Waters Corp.). GC-TOF-MS data were preprocessed using the LECO Chroma TOF™ software (version 4.44; LECO Corp.) and converted into the NetCDF format (\*.cdf) using the LECO Chroma TOF™ software. After conversion, peak detection, retention time correction, and alignment were processed using the MetAlign software package (<http://www.metalign.nl>). The resulting data were exported to an Excel file. Multivariate statistical analysis was processed using SIMCA-P+ (version 12.0, Umetrics; Umea, Sweden). The data sets were auto-scaled (unit variance scaling) and mean-centered in a column-wise fashion. Partial least squares-discriminant analysis (PLS-DA) was performed to compare each data set. The variables were selected based on variable importance in the projection (VIP) value and significant differences were tested by analysis of variance (ANOVA) and Duncan's multiple range tests using PASW Statistics 18 software (SPSS Inc.; Chicago, IL, USA). The clinical and histological results are expressed as mean  $\pm$  standard deviation. Groups were compared with Duncan's multiple range tests.

## 3 Results

### 3.1 Clinical observations and histopathology of mouse skin tissue

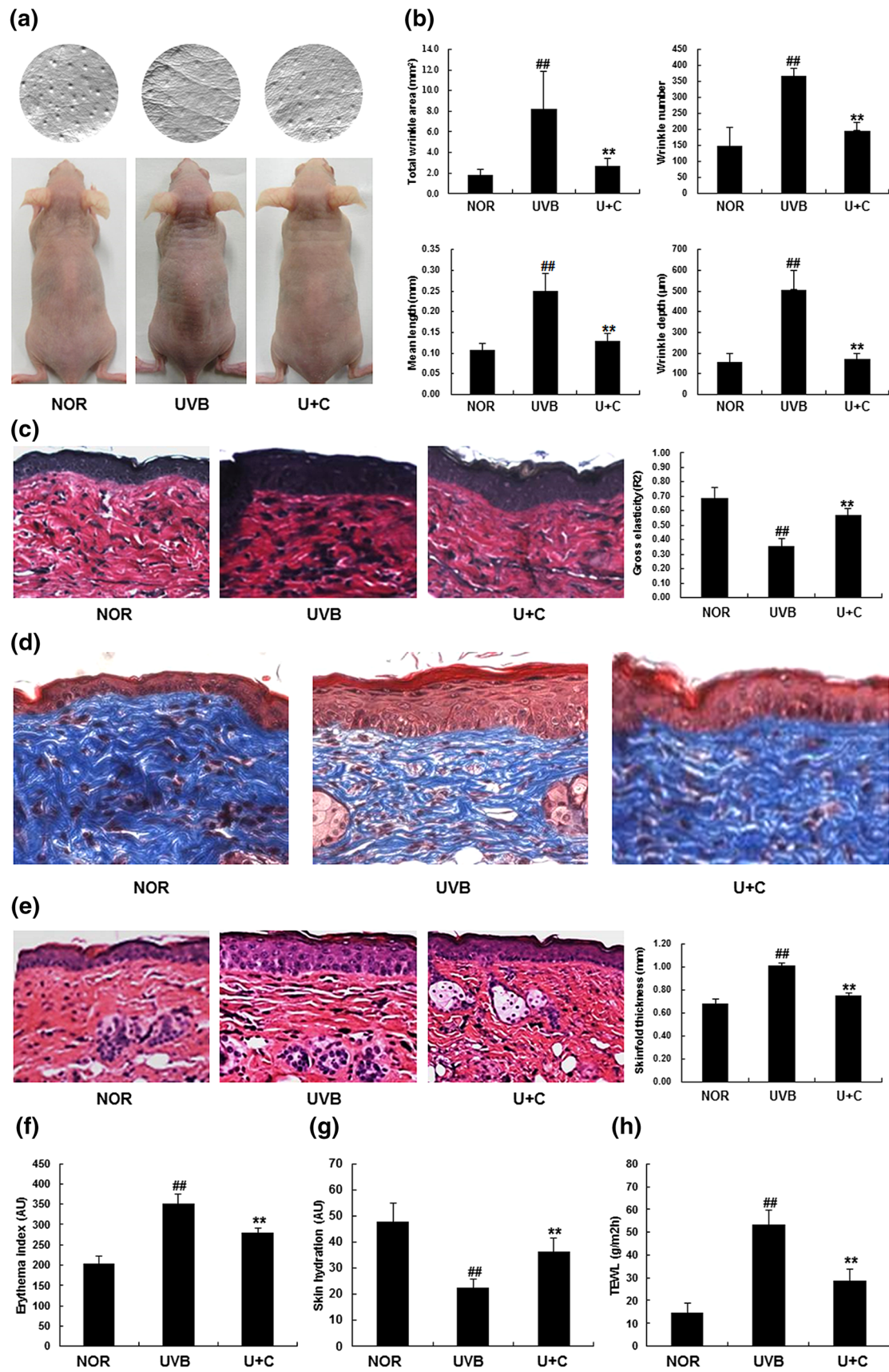
Significant alterations in the histopathology of the mouse skin tissues were observed between the experimental groups. These groups included the NOR group, the UVB group, and the UVB + CGT group. Chronic UVB irradiation for 12 weeks induced severe and deep wrinkles on the dorsal skin of hairless mice (Fig. 1a). The total area, number, mean length, and depth of the wrinkles were increased in the UVB group compared to the NOR group, while the mice in the UVB + CGT group were less affected by UVB irradiation (Fig. 1a and b). Skin thickness, erythema formation, and TEWL were increased in the UVB group compared to the other groups (Fig. 1e, f and h). The gross elasticity, collagen fiber, and skin hydration parameters were reduced by chronic UVB irradiation; however, CGT administration was found to up-regulate these factors (Fig. 1c, d, and g). Overall, chronic UVB

**Fig. 1** Clinical observations of the effects of CGT on UVB-induced mouse skin. **a, b** wrinkle formation; **c** gross elasticity; **d** collagen fibers; **e** skin thickness; **f** erythema index; **g** skin hydration; **h** TEWL. Skin sections are magnified at  $\times 400$ . NOR—NOR group, UVB—UVB group, U + C—UVB + CGT group, ##—represents a significant difference between the NOR and the UVB groups ( $p < 0.01$ ), \*\*—represents a significant difference between the UVB and the UVB + CGT groups ( $p < 0.01$ )

irradiation led to a state of elastosis in the skin of the mice; however, CGT administration to UVB-irradiated mice appeared to inhibit the appearance of this state (Fig. 1c).

### 3.2 Comprehensive metabolite profiling of mouse skin using UPLC-Q-TOF-MS and GC-TOF-MS, and ceramide analysis by NanoMate-LTQ

Primary and secondary metabolites of mouse skin were analyzed using GC-TOF-MS and UPLC-Q-TOF-MS. Multivariate analysis was performed to compare metabolite differences between the experimental groups using PLS-DA models (Fig. 2c and d). For quality control (QC), eight random mixtures of all the samples were injected after every six or seven samples as a means to select outlying samples. The quality of PLS-DA models was evaluated by  $R^2X_{(cum)}$ ,  $R^2Y_{(cum)}$ , and  $Q^2_{(cum)}$ , indicating the fitness and prediction accuracy and they were shown together in the figures. According to the PLS-DA score plots of the UPLC-Q-TOF-MS and GC-TOF-MS data sets (Fig. 2c and d), the NOR group, the UVB group, and the UVB + CGT group were all clearly discriminated from each other. Similar discrimination patterns were shown in PCA score plots (Fig. 2a and b). The NOR group and the UVB group were clearly separated by PLS 1 (17.1 and 17.9 %, respectively), meaning that UVB irradiation affected skin metabolites. The UVB + CGT group was separated from both the NOR group and the UVB group along PLS 2 (10.4 and 12.3 %, respectively); furthermore, the tendency of movement of the UVB + CGT group from the UVB group to the NOR group, was shown on three-dimensional PLS-DA plots. To select the major variables between the experimental groups, both VIP 1 and VIP 2 values ( $>0.7$ ) of the PLS-DA were used. The VIP value is an important parameter for the detection of potential biomarker candidates which reflects the correlation of the metabolites to different biological states. From UPLC-Q-TOF-MS data sets, 24 metabolites, including lysophospholipids and fatty acids, were identified (Table 1). Assignment of metabolites was carried out using the Human Metabolome Database (HMDB) (<http://www.hmdb.ca/>), high resolution mass data (ppm), commercial standard compounds, and references. With this information, relative levels of metabolites were converted into fold changes, which were also presented in Table 1. Fifty-two



metabolites were identified from GC-TOF-MS data sets, and these fell into the categories of amino acids, organic compounds, fatty acids, lipids, nucleobases, and carbohydrates. These metabolites were assigned based on reference to commercial standard compounds and the National Institutes of Standards and Technology library, and their fold changes are summarized in Table 2.

In case of skin ceramides, they were specifically analyzed using Nano-Mate-LTQ, because the detection of ceramides with LC-MS is very different depending on extraction solvents and mobile phases. By Nano-Mate-LTQ, targeted MS/MS spectra were obtained within short analyzing time (2 min), which provided information regarding the specific fragment ions of the acyl- and

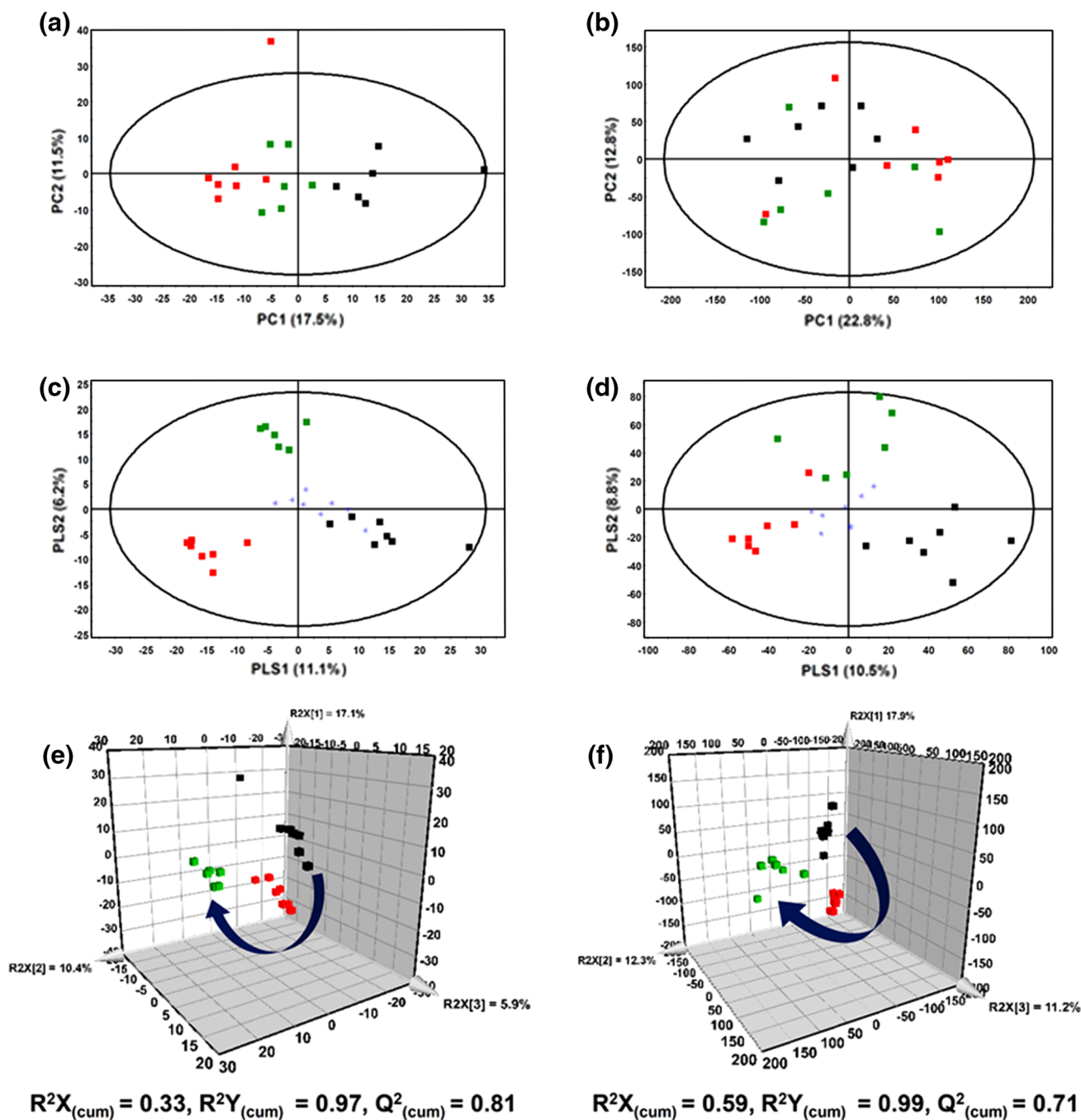


**Fig. 2** The PCA score scatter plots (a), (b) and PLS-DA score scatter plots (c), (d), (e), (f) of mouse skin tissue extracts analyzed by UPLC-Q-TOF-MS (a), (c), (e) and GC-TOF-MS (b), (d), (f). c, d—QC

samples-containing PLS-DA score plot; e, f—Three-dimensional PLS-DA score plot. *Black Filled square*—NOR group; *Red filled square*—UVB group; *Green filled square*—UVB + CGT group

**Table 1** The major mouse skin metabolites altered by chronic UVB irradiation and CGT administration, as identified by UPLC-Q-TOF-MS analysis

Tentative metabolites	$t_R$ (min)	Measured MS ( $m/z$ )	HMDB formular	PPM <sup>b</sup>	Adduct	Fold change (UVB/NOR)	Fold change (UVB + GTE/UVB)
LysoPC (16:1)*	7.57	478.2930	C <sub>24</sub> H <sub>48</sub> NO <sub>7</sub> P	0.3	[M-CH <sub>3</sub> ] <sup>-</sup>	1.20 <sup>#</sup>	0.91
LysoPC (18:0)*	9.95	508.3400	C <sub>26</sub> H <sub>54</sub> NO <sub>7</sub> P	3.2	[M-CH <sub>3</sub> ] <sup>-</sup>	0.87 <sup>#</sup>	1.13 <sup>#</sup>
LysoPC (18:0)*	10.29	508.3409	C <sub>26</sub> H <sub>54</sub> NO <sub>7</sub> P	2.5	[M-CH <sub>3</sub> ] <sup>-</sup>	0.94 <sup>#</sup>	1.11 <sup>#</sup>
LysoPC (18:2)*	7.78	504.3079	C <sub>26</sub> H <sub>50</sub> NO <sub>7</sub> P	-1.8	[M-CH <sub>3</sub> ] <sup>-</sup>	1.52 <sup>#</sup>	0.88
LysoPC (18:2)*	8.02	504.3062	C <sub>26</sub> H <sub>50</sub> NO <sub>7</sub> P	-2.6	[M-CH <sub>3</sub> ] <sup>-</sup>	1.37 <sup>#</sup>	0.88
LysoPC (22:6)*	7.74	552.3099	C <sub>30</sub> H <sub>50</sub> NO <sub>7</sub> P	-0.5	[M-CH <sub>3</sub> ] <sup>-</sup>	0.74	1.54 <sup>#</sup>
LysoPE (18:1)*	8.67	478.2943	C <sub>23</sub> H <sub>46</sub> NO <sub>7</sub> P	1.3	[M-H] <sup>-</sup>	1.35 <sup>#</sup>	1.04
LysoPE (18:1)*	8.95	478.2925	C <sub>23</sub> H <sub>46</sub> NO <sub>7</sub> P	-1.9	[M-H] <sup>-</sup>	1.20 <sup>#</sup>	1.06
LysoPE (18:2)*	7.73	476.2787	C <sub>23</sub> H <sub>44</sub> NO <sub>7</sub> P	2.2	[M-H] <sup>-</sup>	1.74 <sup>#</sup>	0.82
LysoPE (18:2)*	7.97	476.2776	C <sub>23</sub> H <sub>44</sub> NO <sub>7</sub> P	2.2	[M-H] <sup>-</sup>	1.56 <sup>#</sup>	0.86
LysoPE (20:0)*	9.24	494.3262	C <sub>25</sub> H <sub>52</sub> NO <sub>7</sub> P	3.8	[M-CH <sub>3</sub> ] <sup>-</sup>	1.74 <sup>#</sup>	0.99
LysoPE (20:0)*	9.44	494.3250	C <sub>25</sub> H <sub>52</sub> NO <sub>7</sub> P	1.6	[M-CH <sub>3</sub> ] <sup>-</sup>	1.28 <sup>#</sup>	0.99
Docosahexaenoic acid	11.17	327.2326	C <sub>22</sub> H <sub>32</sub> O <sub>2</sub>	-1.1	[M-H] <sup>-</sup>	0.76 <sup>#</sup>	1.33 <sup>#</sup>
Oxodecanoic acid or hydroxydecanoic acid	11.31	297.2415	C <sub>18</sub> H <sub>34</sub> O <sub>3</sub>	-0.6	[M-H] <sup>-</sup>	1.21 <sup>#</sup>	1.08
Arachidonic acid	11.46	303.2325	C <sub>20</sub> H <sub>32</sub> O <sub>2</sub>	0.3	[M-H] <sup>-</sup>	0.87 <sup>#</sup>	1.00
Linoleic acid	11.68	279.2320	C <sub>18</sub> H <sub>32</sub> O <sub>2</sub>	0.5	[M-H] <sup>-</sup>	0.68 <sup>#</sup>	1.07
Octadecenoic acid	12.69	281.2468	C <sub>18</sub> H <sub>34</sub> O <sub>2</sub>	-1.9	[M-H] <sup>-</sup>	0.80 <sup>#</sup>	1.00

Metabolites selected by VIP > 0.7 from PLS-DA model

HMDB The Human Metabolome Data Base (<http://www.hmdb.ca/>), LysoPC lysophosphatidylcholine, LysoPE lysophosphatidylethanolamine,  $t_R$  retention time

\* Regioisomers of LysoPC and LysoPE

#  $p$  value < 0.05

<sup>a</sup> Assignment of metabolites was carried out using HMDB, high resolution mass data (ppm), and references. Docosahexaenoic acid, arachidonic acid, and linoleic acid were identified with commercial standard compound

<sup>c</sup> Mass tolerance from elemental composition analysis of MassLynx software

sphingoid-units. Using synthetic ceramide standards, and our in-house skin ceramide MS/MS database (Shin et al. 2014), 32 ceramides were identified, including five types (AS, NP, NS, NH, and NdS). The information regarding these ceramides is summarized in Table S1.

### 3.3 Effects of CGT administration on UVB-induced mouse skin metabolite changes

As shown in Tables 1, 2 and Table S1, numerous metabolites, including amino acids, carbohydrates, nucleobases, organic compounds, fatty acids, lipids, lysophospholipids, and ceramides, were affected by CGT administration in UVB-irradiated mouse skin. With the exception of stearyl- and docosahexaenoyl-lysophosphatidylcholines (lysoPCs), the amino acids, ceramides, remaining lysophospholipids, and several organic acids, were increased in the UVB group compared to the NOR group. These increase were reduced in the UVB + CGT group as compared to the UVB group. On

the contrary, fatty acids, lysoPCs, and carbohydrates were decreased by UVB irradiation, and it also attenuated upon CGT administration. In case of the nucleobases, they were not significantly altered by UVB irradiation, but they were significantly changed in the UVB + CGT group compared to the UVB group. Among the assigned metabolites, several showed remarkable changes compared to others upon UVB irradiation and CGT administration. Ascorbic acid showed a dramatic increase of 2.09-fold in the UVB group compared with the NOR group, and decreased by 0.37-fold in the UVB + CGT group compared with the UVB group. Malonic acid also showed a 1.39-fold increase and a 0.61-fold decrease in the UVB and UVB + CGT groups, respectively. Conversely, the lactose level was notably decreased by 0.48-fold by UVB irradiation, and increased by 2.12-fold with CGT administration. In the cases of inosine and hypoxanthin alterations by UVB irradiation were insignificant, but they decreased significantly (by 0.43- and 0.32-fold, respectively) in the UVB + CGT group compared to the UVB group.

**Table 2** The major mouse skin metabolites altered by chronic UVB irradiation and CGT administration, as analyzed by GC-TOF-MS

Metabolites <sup>a</sup>	$t_R$ (min)	Identified ion ( $m/z$ )	Fold change (UVB/NOR)	Fold change (UVB + GTE/UVB)
Amino acids				
Threonine	8.12	219	1.11*	0.97
Citrulline	8.73	128	1.39*	0.82
Glutamic acid	10.04	246	1.11*	0.94
Asparagine	10.45	116	1.17*	1.04
Lysine	10.69	84	1.84*	0.67
Ornithine	11.52	142	1.56*	0.92
Tyrosine	12.35	218	1.09*	0.97
Organic compounds				
Oxalic acid	5.58	190	1.16	1.61*
Malonic acid	8.98	223	1.39*	0.61*
Hypotaurine	9.92	188	1.25*	0.88
Hypoxanthine	11.46	265	1.03	0.43*
Ascorbic acid	12.46	332	2.09*	0.37*
Fatty acids				
Myristic acid	11.63	117	0.65*	1.14
Palmitoleic acid	12.81	117	0.53*	1.32
Palmitic acid	12.93	117	0.74*	1.04
Linoleic acid	13.95	337	0.64*	1.12
Oleic acid	13.98	339	0.64*	1.13
Arachidonic acid	14.86	91	0.81*	1.06
Docosahexaenoic acid	15.87	117	0.59*	1.43
Nucleosides and its derivatives				
Uracil	7.67	99	1.30*	1.09
Uridine	15.39	217	1.23	0.71*
Inosine	16.04	230	1.33	0.32*
Carbohydrates				
Glycerol	7.06	117	0.85*	0.98
Mannose	12.08	319	0.81*	1.17
myo-Inositol	13.41	217	0.77*	0.99
Lactose	16.75	204	0.48*	2.12*

 $t_R$  retention time\*  $p$  value < 0.05<sup>a</sup> Metabolites selected by VIP > 0.7 from PLS-DA model, and identified with commercial standard compounds (STD)

#### 4 Discussion

In this study, we employed green tea consisting high contents of catechin (27.58 %), for oral administration in mice to examine the effects of CGT on alteration of mouse skin morphology and metabolites caused by chronic UVB irradiation. Our clinical observations showed that chronic UVB irradiation caused skin abnormalities, including wrinkling, erythema, dryness, epidermal thickness, elastosis, and disorganization of collagen fibers, whereas CGT administration significantly attenuated these skin alterations (Fig. 1). These results with prevention of UVB-induced skin abnormality by CGT were consistent with those of previous researches (Katiyar and Mukhtar 2001; Vayalil et al. 2004). Based on these results, we also revealed that CGT administration attenuated UVB-induced alteration of skin metabolites through MS-based

metabolomics approaches and target-analysis of skin ceramides using Nano-Mate-LTQ.

In our study, ceramides, fatty acids, and lysophospholipids were detected which are constituent of stratum corneum (SC). The SC is the outer epidermal layer of the skin, and plays an important role in permeability barrier homeostasis. The SC consists mainly of ceramides, cholesterol, fatty acids, and minor components such as phospholipids (Feingold 2007). When the skin exposure to chronic UVB irradiation, the SC lipids structure was disrupted, this leads to wrinkle formation and alteration of SC lipids contents. We also observed the levels of SC lipids such as ceramides and lysophospholipids were increased and those of fatty acids were decreased by UVB irradiation. The attenuation of these altered metabolites was shown upon CGT administration. Wefers et al. (1991) revealed that level of skin ceramides were increased by UVB



radiation. On the other hand, there are conflicting opinions on changes of fatty acid contents by UVB irradiation. Wefers et al. (1991) reported that amounts of free fatty acids significantly increased in human skin by UVB irradiation for 3 weeks, whereas Kim et al. (2010) revealed those significantly decreased by both acute and chronic UVB irradiation. These differences were might be due to different conditions of experiments such as period and dosage of UVB exposure. In the case of cholesterol, it was detected, but not selected as major variable in our results. However, when comparing relative cholesterol levels measured by GC-TOF-MS, it showed a decrease of 0.95-fold by UVB radiation, an increase of 1.12-fold by CGT administration. Although their alterations were not significant, alteration patterns of relative levels were consistent with other study (Meguro et al. 1999). From these results, we confirmed that chronic UVB irradiation induced SC lipids alteration, and then CGT inhibited these alterations.

Chronic UVB irradiation also reduces skin moisturization. Some studies reported that total content of free amino acids, the primary natural moisturizing factors in the SC, contributes to water holding capacity (Katagiri et al. 2003; Rawlings and Harding 2004). Yahagi et al. (2011) reported that lysoPCs improve the skin moisturizing capability by up-regulation of mRNA encoding important components of skin hydration. Skin metabolites including amino acids, lysoPCs, ceramides, and glycerol were altered by UVB irradiation in our study. Together, these metabolites alterations were reduced by CGT administration. There was a research that EGCG supplementation strengthened skin tolerance and prevented disturbance of skin barrier function induced by chronic UVB irradiation (Jeon et al. 2009). Therefore, we could suggest that overall attenuations of skin hydration-related metabolites by CGT were involved in an increase on water holding capacity such as TEWL and skin hydration.

Among these altered metabolites by UVB irradiation, lysophospholipids and fatty acids were also highly related to skin inflammation which led to cause erythema on skin. LysoPC is known to induce erythema and inflammation in the skin (Ryborg et al. 2000), and fatty acids affect the inflammatory process via various cellular signaling mechanisms (Calder 2011). In Fig. 1, erythema was significantly attenuated by CGT administration, which means that CGT highly reduced UVB-induced skin inflammation. The effects of green tea catechins on UVB-induced inflammation have been well-studied; Katiyar and Mukhtar (2001) reported that the treatment of mouse skin with the EGCG prevented UVB-induced infiltration of leukocytes and antigen-presenting cells. Moreover, Meeran et al. (2009) revealed drinking green tea polyphenol inhibited UVB-induced inflammation through reduction of cyclooxygenase-2 expression.

Among all the metabolites, ascorbic acid and lactose levels were most remarkably changed by UVB irradiation and significantly attenuated by CGT administration, particularly. Generally, ascorbic acid and some oligosaccharides were known to have connection with skin connective tissues such as collagen (Chan 1993; Bertin et al. 2008). Ascorbic acid acts as a regulator in collagen biosynthesis (Murad et al. 1981). Oligosaccharides such as lactose, melibiose, and stachyose can prevent the symptoms of connective tissue aging related with a protease of the elastase from human fibroblasts (Bertin et al. 2008). Degradation of skin connective tissues mostly is mediated by matrix metalloproteinases (MMPs) and then causes deep wrinkle formation in skin. MMPs are induced by UVB irradiation (Brenneisen et al. 2002; Bae et al. 2010). EGCG of green tea prevents collagen degradation, and the induction of MMP expression in photodamaged skin (Vayalil et al. 2004; Bae et al. 2008). Based on this literature, our results with the increase of collagen fiber production and elasticity as well as the reverse of ascorbic acid and lactose levels by CGT administration, suppose that CGT partially influences on maintaining of skin collagen by regulating the production of ascorbic acid and lactose.

Skin biomolecules, including aromatic amino acids, nucleic acids, and urocanic acid, act as radiation absorbents in the UVB range (Svobodova et al. 2006; Bae et al. 2008). These metabolites are directly damaged by UVB irradiation or interact with UVB-induced reactive oxygen species (ROS) causing oxidative damage (Svobodova et al. 2006). The ROS induces DNA damage by formation of cyclobutane pyrimidine dimers and pyrimidine(6-4)pyrimidone dimers (Nichols and Katiyar 2010). In our data, the levels of 3 nucleosides (uracil, uridine, and inosine) showed a tendency to increase by UVB irradiation, which demonstrated that the changed level of these metabolites might influence on ROS production in part. There was opposite results were reported that the levels of hypoxanthine and inosine were decreased by UVB irradiation (Park et al. 2014). However, the number and altered levels of skin metabolites could be different depending on period and dosage of UVB irradiation. In case of inosine and hypoxanthine, they were remarkably decreased by CGT administration in this study. According to previous reports, green tea catechins are effective in inhibiting ROS production and DNA damage (Yang et al. 2009; Nichols and Katiyar 2010). However, the research with the direct relationship between nucleosides and green tea has not well-studied. Nevertheless, from these results, we cautiously propose that CGT administration inhibit ROS production and may affect the level of these metabolites related with ROS production.

Based on our results with the changes of mouse skin metabolites caused by UVB irradiation and its attenuations

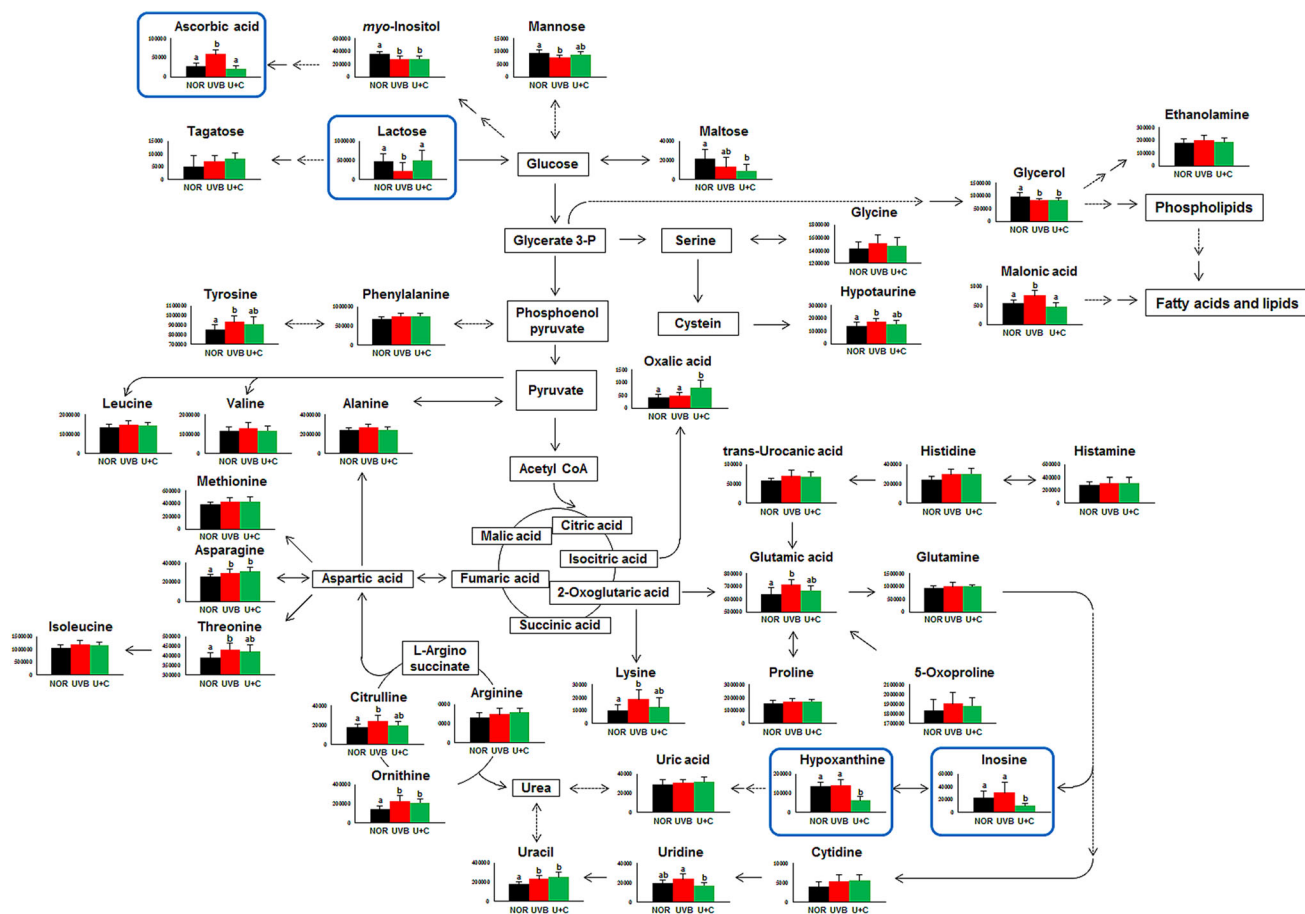


**Fig. 3** A schematic diagram of the proposed metabolic pathway based on the changes of mouse skin metabolites caused by UVB irradiation and its attenuations according to CGT administration. The different letters indicate significant differences as determined by ANOVA followed by Duncan's multiple range tests ( $p < 0.05$ ). The

dashed line indicates multiple steps. Black Filled square—NOR group; Red filled square—UVB group; Green filled square—UVB + CGT group. Blue square boxes indicate biomarker candidates to explain CGT effects on UVB-irradiated skin

according to CGT administration, we proposed a metabolic pathway using major variables in our data analysis (Fig. 3). This metabolic pathway might help a better understanding of the relationship between skin metabolites altered by UVB irradiation and the effects of CGT administration. However, direct relationships between the altered skin metabolites and CGT administration are yet to be established to determine any molecular mechanisms at work. Therefore, further investigation through biochemical and molecular studies will be required to fully evaluate our results.

## 5 Concluding remarks

In this study, we revealed the remarkable attenuation of both clinical observations and alterations of numerous metabolite levels using MS-based metabolomics approach upon CGT administration in UVB-irradiated mice skin.

These overall changes in skin metabolites could be highly relevant to observed changes in skin condition, i.e., thickness, hydration, collagen fiber, and wrinkle content. Among the metabolites, purine nucleosides (inosine and hypoxanthine), ascorbic acid, and lactose showed most remarkable changes. We suggest that they could be biomarker candidates to explain CGT effects on UVB-irradiated skin. To the best of our knowledge, this study was the first attempt to investigate the effects of CGT administration on UVB-irradiated mouse skin, using a metabolomics approach.

**Acknowledgments** This study was supported by a grant of the Korea Health Technology R&D Project, Ministry of Health & Welfare, Republic of Korea (Grant No.: HN13C0076) and of the Cooperative Research Program for Agricultural Science & Technology Development, Rural Department Administration, Republic of Korea. (No.: PJ 009826).

**Conflict of interest** The all authors declared that they have no conflict of interest in the submission of this manuscript.

**Compliance with Ethics Requirements** All procedures performed in studies involving animals were in accordance with ethical standards of the institution or practice at which the studies were conducted.

## References

- Arakaki, A. K., Skolnick, J., & McDonald, J. F. (2008). Marker metabolites can be therapeutic targets as well. *Nature*, *456*, 443.
- Bae, J. Y., Choi, J. S., Choi, Y. J., et al. (2008). (–)Epigallocatechin gallate hampers collagen destruction and collagenase activation in ultraviolet-B-irradiated human dermal fibroblasts: Involvement of mitogen-activated protein kinase. *Food and Chemical Toxicology*, *46*, 1298–1307.
- Bae, J. Y., Choi, J. S., Kang, S. W., Lee, Y. J., Park, J., & Kang, Y. H. (2010). Dietary compound ellagic acid alleviates skin wrinkle and inflammation induced by UV-B irradiation. *Experimental Dermatology*, *19*, e182–e190.
- Bertin, C., Zunino, H., Lanctin, M., et al. (2008). Combined retinol-lactose-glycolic acid effects on photoaged skin: A double-blind placebo-controlled study. *International Journal of Cosmetic Science*, *30*, 175–182.
- Brenneisen, P., Sies, H., & Scharffetter-Kochanek, K. (2002). Ultraviolet-B irradiation and matrix metalloproteinases: From induction via signaling to initial events. *Annals of the New York Academy of Sciences*, *973*, 31–43.
- Calder, P. C. (2011). Fatty acids and inflammation: The cutting edge between food and pharma. *European Journal of Pharmacology*, *668*, s50–s58.
- Chan, A. C. (1993). Partners in defense, vitamin E and vitamin C. *Canadian Journal of Physiology and Pharmacology*, *71*, 725–731.
- Feingold, K. R. (2007). The role of epidermal lipids in cutaneous permeability barrier homeostasis. *The Journal of Lipid Research*, *48*, 2531–2546.
- Huang, S. M., Chang, Y. H., Chao, Y. C., & Lin, J. A. (2013). EGCG-rich green tea extract stimulates sRAGE secretion to inhibit S100A 12-RAGE axis through ADAM1-mediated ectodomain shedding of extracellular RAGE in type 2 diabetes. *Molecular Nutrition & Food Research*, *57*, 2264–2268.
- Jeon, S. E., Choi-Kwon, S., Park, K. A., et al. (2003). Dietary supplementation of (+)-catechin protects against UVB-induced skin damage by modulating antioxidant enzyme activities. *Photodermatology, Photoimmunology and Photomedicine*, *19*, 235–241.
- Jeon, H. Y., Kim, J. K., Kim, W. G., & Lee, S. J. (2009). Effects of oral epigallocatechin gallate supplementation on the minimal erythema dose and UV-induced skin damage. *Skin Pharmacology and Physiology*, *22*, 137–141.
- Katagiri, C., Sato, J., Nomura, J., & Denda, M. (2003). Changes in environmental humidity affect the water-holding property of the stratum corneum and its free amino acid content, and the expression of filaggrin in the epidermis of hairless mice. *Journal of Dermatological Science*, *31*, 29–35.
- Katiyar, S. K., & Mukhtar, H. (2001). Green tea polyphenol (–)-epigallocatechin-3-gallate treatment to mouse skin prevents UVB-induced infiltration of leukocytes, depletion of antigen-presenting cells, and oxidative stress. *Journal of Leukocyte Biology*, *69*, 719–726.
- Kim, J., Choi, J. N., Choi, J. H., Cha, Y. S., Muthaiya, M. J., & Lee, C. H. (2013). Effect of fermented soybean product (Cheonggukjang) intake on metabolic parameters in mice fed a high-fat diet. *Molecular Nutrition & Food Research*, *57*, 1886–1891.
- Kim, E. J., Jin, X. J., Kim, Y. K., et al. (2010). UV decreases the synthesis of free fatty acids and triglycerides in the epidermis of human skin in vivo, contributing to development of skin photoaging. *Journal of Dermatological Science*, *57*, 19–26.
- Kligman, L. H., Akin, F. J., & Kligman, A. M. (1985). The contributions of UVA and UVB to connective tissue damage in hairless mice. *The Journal of Investigative Dermatology*, *84*, 272–276.
- Meeran, S. M., Akhtar, S., & Katiyar, S. K. (2009). Inhibition of UVB-induced skin tumor development by drinking green tea polyphenols is mediated through DNA repair and subsequent inhibition of inflammation. *The Journal of Investigative Dermatology*, *129*, 1258–1270.
- Meguro, S., Arai, Y., Masukawa, K., Uie, K., & Tokimitsu, I. (1999). Stratum corneum lipid abnormalities in UVB-irradiated skin. *Photochemistry and Photobiology*, *69*, 317–321.
- Mukhtar, H., & Ahmad, N. (2000). Tea polyphenols: prevention of cancer and optimizing health. *The American Journal of Clinical Nutrition*, *71*, S1698–S1702.
- Murad, S., Grove, D., Lindberg, K. A., Reynolds, G., Sivarajah, A., & Pinnell, S. R. (1981). Regulation of collagen synthesis by ascorbic acid. *Proceedings of the National Academy of Sciences of the United States of America*, *78*, 2879–2882.
- Nagao, T., Hase, T., & Tokimitsu, I. (2007). A Green tea extract high in catechins reduces body fat and cardiovascular risks in humans. *Obesity*, *15*, 1473–1483.
- Nichols, J. A., & Katiyar, S. K. (2010). Skin photoprotection by natural polyphenols: anti-inflammatory, antioxidant and DNA repair mechanisms. *Archives of Dermatological Research*, *302*, 71–83.
- Park, H. M., Shin, J. H., Kim, J. K., et al. (2014). MS-based metabolite profiling reveals time-dependent skin biomarkers in UVB-irradiated mice. *Metabolomics*, *10*, 663–676.
- Rawlings, A. V., & Harding, C. R. (2004). Moisturization and skin barrier function. *Dermatologic Therapy*, *17*, 43–48.
- Ryborg, A. K., Deleuran, B., Sogaard, H., & Kragballe, K. (2000). Intracutaneous injection of lysophosphatidylcholine induces skin inflammation and accumulation of leukocytes. *Acta Dermatovenereologica*, *80*, 242–246.
- Shin, J. H., Shon, J. C., Lee, K., et al. (2014). A lipidomic platform establishment for structural identification of skin ceramide with non-hydroxyacyl chains. *Analytical and Bioanalytical Chemistry*, *406*, 1917–1932.
- Svobodova, A., Walterova, D., & Vostalova, J. (2006). Ultraviolet light induced alteration to the skin. *Biomedical papers of the Medical Faculty of the University Palacky, Olomouc, Czechoslovakia*, *150*, 25–38.
- Vayalil, P. K., Mittal, A., Hara, Y., Elmets, C. A., & Katiyar, S. K. (2004). Green tea polyphenols prevent ultraviolet light-induced oxidative damage and matrix metalloproteinases expression in mouse skin. *Journal of Investigative Dermatology*, *122*, 1480–1487.
- Wefers, H., Melnik, B. C., Flur, M., Bluhm, C., Lahmann, P., & Plewig, G. (1991). Influence of UV irradiation on the composition of human stratum corneum lipids. *Journal of Investigative Dermatology*, *96*, 959–962.
- Yahagi, S., Koike, M., Okano, Y., & Masaki, H. (2011). Lysophospholipids improve skin moisturization by modulating of calcium-dependent cell differentiation pathway. *International Journal of Cosmetic Science*, *33*, 251–256.
- Yang, C. S., Lambert, J. D., & Sang, S. (2009). Antioxidative and anti-carcinogenic activities of tea polyphenols. *Archives of Toxicology*, *83*, 11–21.
- Zhang, A., Sun, H., Wang, P., Han, Y., & Wang, X. (2012). Recent and potential development of biofluid analyses in metabolomics. *Journal of Proteomics*, *75*, 1079–1088.
- Zhou, M., Wang, S., Zhao, A., et al. (2012). Transcriptomic and metabolomic profiling reveal synergistic effects of Quercetin and Resveratrol supplementation in high fat diet fed mice. *Journal of Proteome Research*, *11*, 4961–4971.